JOURNAL OF MATERIALS SCIENCE **38** (2003) 1021 – 1032

Failure mechanisms in viscoelastic films

J. A. F. HARVEY, D. CEBON
Engineering Department, Cambridge University, Trumpington St., Cambridge, CB2 1PZ, UK
E-mail: dc@eng.cam.ac.uk

This paper presents the results of tensile tests on viscoelastic films of two materials: a 100 pen bitumen and a commercial corn syrup. Experiments were performed using double-cantilever beam specimens, and butt-joint specimens, for a wide range of testing conditions. Failure by brittle fracture, voiding, and various viscous flow mechanisms was observed. The results are presented in the form of maps and are discussed in conjunction with appropriate mathematical models. © *2003 Kluwer Academic Publishers*

Nomenclature

a	Critical flaw size
A	Aspect ratio of film
A^*	Critical aspect ratio of film
E	Young's modulus
F	Force
G	Strain energy release rate
G_{IC}	Critical strain energy release rate
h	Half film thickness
h^*	Half thickness of ligament with the critical aspect ratio
n	Power law exponent
Q	Activation energy (constant)
R	General gas constant
r_0	Initial film radius
r_0^*	Diameter of ligament with the critical aspect ratio
r_0'	Ligament radius in voided film
T	Temperature
T_0	Reference temperature (constant)
α	Material constant in rheological model
β	Material constant in rheological model
$\dot{\varepsilon}$	Direct strain rate
ε_n	Nominal strain
$\dot{\varepsilon}_0$	Reference strain rate (constant)
$\dot{\varepsilon}_T$	Temperature-compensated strain rate
ν	Poisson's ratio
σ	Direct stress
σ_0	Reference stress (constant)
ψ	Film stiffening factor

1. Introduction

When an elastic thin film is placed in tension, the stress-state is no longer uniaxial due to the geometrical constraint, and the stress distribution within the material is in general non-uniform. Kinloch [1] noted that if both the adhesive and the adherend had the same tendency to deform laterally, there would be no constraint.

As the film gets thinner, there is a stiffening effect, giving rise to an effective Young's modulus, E_e. For a thin axisymmetric, incompressible film, with an assumed parabolic stress distribution, Nadai [2] showed that

$$E_e = \frac{A^2 E}{8},$$

where E is the Young's modulus of the film material and A is the aspect ratio (diameter/thickness) of the film. This stiffening effect is most pronounced for incompressible films.

The key role of the Poisson's ratio of the adhesive layer, υ_a, in determining the joint stress distribution was illustrated by Holownia [3]. A lower value of υ_a causes the stress field near the centre of the joint to be less parabolic and more uniform. Harrison and Harrison [4] asserted and that for joints of aspect ratio 10 or more, and υ_a of 0.49 or less, the stress field in normalised coordinates is independent of aspect ratio. Further they predicted, using a finite element analysis, that the stress field is uniform up to a radius of five film thicknesses from the edge of the joint.

For adhesives with high Poisson's ratio, the joint stresses are very sensitive to aspect ratio. This is because incompressibility acts as a constraint in addition to the geometrical constraint created by interface friction. In fact, pure hydrostatic tension can only be achieved in the centre of a film if υ_a is 0.5. However, for practical purposes, close to hydrostatic conditions are obtained for lower Poisson's ratios.

Cottrell [5], analysed the stress in a thin film of linear viscous material. Cheung and Cebon [6] derived solutions for the stresses in thin films of non-linear (power-law) viscous and viscoelastic materials in compression. These solutions are discussed later.

The constitutive response of viscoelastic materials depends on stress level, duration of loading and temperature [7]. The glass transition temperature defines the change in the properties of (thermoplastic) polymers from ductile to brittle. At temperatures far above glass transition, an un-crosslinked polymer is expected to behave like a liquid, exhibiting flow [8]. This is also the case at very low strain rates. Below the glass transition temperature, or at very high strain rates, brittle

fracture is common. For polymers of high molecular weight, fracture can take the form of crazing, in which long molecular chains bridge the crack faces within the process zone. This behaviour is rate sensitive and has been modelled, for example by Chudnovsky *et al*. [9]. However, some polymers, e.g. bitumen have short molecular chains and do not display crazing. Work by Genin and Cebon [10] revealed that the mechanism of tensile failure in bitumen is either brittle fracture or void growth and coalescence, depending on the conditions of temperature and strain rate.

For ductile joints, instead of cracking, the film material flows inward from the edge, particularly in materials of low porosity and high Poisson's ratio [11, 12]. Gent and Lindley [13] observed cavitation in ductile rubber joints; where the number of cavities increased, and the size of cavities decreased with rising aspect ratio. Blatz and Kakavas [14], by studying the lateral deformation of their butt joints, presented an analysis for determining the effective Poisson's ratio, as a measure of void content.

Ductile failure in butt joints is either defined at the point of void nucleation, the point of peak stress, or the point of final rupture. For example, the nominal stress-strain curves of Gent and Lindley [13] levelled off during void nucleation in a rubber film. After this the load continued to rise until final rupture.

Experiments show that the nominal failure stress of axially loaded butt joints increases with declining film thickness. Kinloch [1] stated that this is the case for a wide range of polymeric adhesives from epoxies to silicone materials. Adams and Coppendale [15] made a similar observation with regard to the yield stress of ductile butt joints compared to uniaxial specimens. Based on a von Mises yield criterion, the ratio of thin film to uniaxial yield stress was also predicted to increase with rising Poisson's ratio.

Adams and Coppendale [15] noted however, that the failure stress of brittle butt joints was lower than that of brittle uniaxial specimens, because of the presence of stress concentrations in the joints. The most common failure criterion for brittle butt joints is the critical interfacial stress concentration factor [16]. The tests of Dukes and Bryant [17] showed where the fracture stress in joints with thicker films was lower than that in thinner films. They suggested that the greater statistical likelihood of large flaws in the thick films was the reason for this. Kinloch [1] hypothesised that the thin film stiffening effect was responsible for this rise in failure stress with aspect ratio.

Viscous 'fingering' is associated with the flow of a viscous liquid in the narrow gap between parallel plates. It is sensitive to strain-rate. Viscous fingering was first recorded by Saffman and Taylor [18, 19]. A viscous liquid was constrained within a narrow gap between two fixed plates, creating a 'Hele-Shaw cell'. This test liquid was displaced by an incoming flow from one edge. The fluid-fluid interface, being imperfect, had perturbations which developed a finger-like appearance, as the lower viscosity fluid displaced the test liquid. This was because the maximum pressure gradient between the two fluids was located at the extreme tip of the perturbations, and this caused them to grow in an unstable manner. At low strain rates, a smooth finger shape is developed. With increasing strain rate, the wavelength falls and the initial fingers become thinner. At high strain rates, the fingers also subdivide, giving a dendritic pattern. In the viscoelastic fluids tested by Maher and Ignes-Mullol [20], fracture-type behaviour was observed at very high strain rates, and very narrow needle-like fingers of an unstable nature were seen. Fields and Ashby [21] studied finger-like crack growth in linear and non-linear viscous films with the geometries similar to those of butt joints and peel joints. The invading fluid was air at atmospheric pressure, which displaced a film of glycerine.

This paper investigates the mechanisms of failure in thin films of two viscoelastic materials: bitumen and corn syrup. The objective was to map-out and interpret the behaviour over a broad range of loading conditions. The motivation for the work was to develop an understanding of the fracture mechanisms that take place within asphalt road surfaces. Asphalt is a complex composite, consisting of a high volume fraction of stiff aggregate particles, bound by thin films of (filled) bitumen. During Mode I cracking, the bitumen film between two aggregate particles is loaded in tension, and the bitumen-aggregate contact can be idealised as an adhesive joint between two stiff adherends. This defined the specimen configuration used in the tests. Corn syrup was used because it has similar viscous properties to bitumen, but is transparent - facilitating visualisation of the failure mechanisms.

2. Fracture tests on bitumen films

An extensive program of tensile testing on bitumen films was conducted to map out the fracture behaviour [22]. Two types of specimens were tested: double cantilever beam joints (DCB's) and butt joints. The form of the DCB joint is sketched in Fig. 1a and the bitumen butt joint used is depicted in Fig. 1b. Tests were also performed with thin films of corn syrup, which is a transparent viscous liquid. Fig. 1c shows the arrangement used to create a butt joint using a film of corn syrup.

Both ductile and brittle behaviour was observed in bitumen, as indicated by the stress-strain curves in Fig. 2. Fig. 2a shows three ductile stress-strain curves, in which the peak stress is rate dependent. Fig. 2b shows two curves associated with brittle fracture, in which the peak stress is rate independent.

In the ductile region, the steady state uniaxial failure stress in bitumen is given by [6]

$$\frac{\dot{\varepsilon}}{\dot{\varepsilon}_0} = \left(\frac{\sigma}{\sigma_0}\right)^n \exp\left(\frac{-Q}{RT}\right), \tag{1}$$

where the reference stress, σ_0, the reference strain rate, $\dot{\varepsilon}_0$, and the activation energy, Q, take the values listed in Table I, for the bitumen studied here. R is the universal gas constant.

A temperature-compensated equivalent strain rate was developed from (1) in [22] to enable comparison of the results of tests at different temperatures and strain rates. The temperature-compensated strain rate is

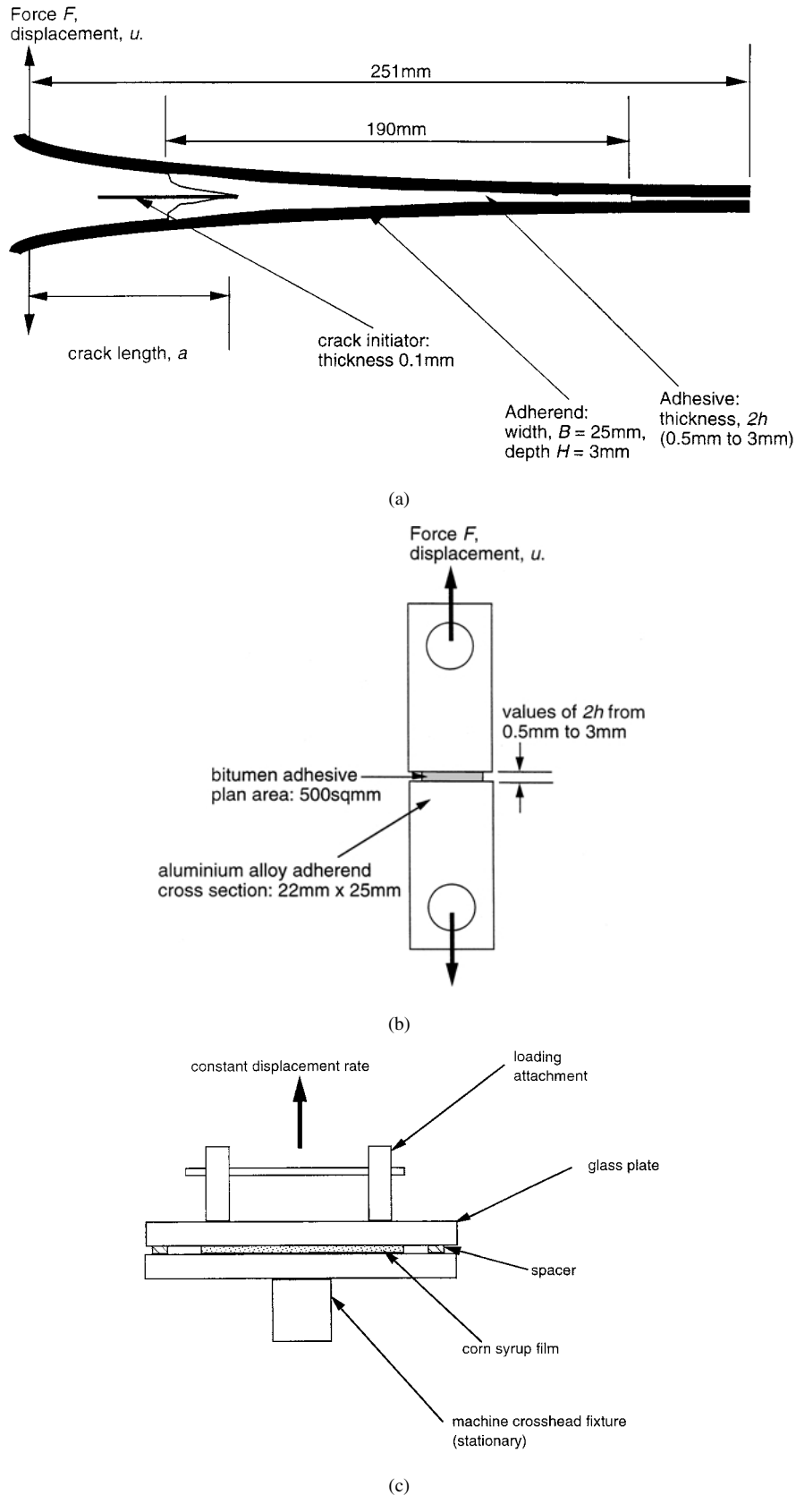

Figure 1 (a) Diagram of a DCB specimen during testing, (b) Diagram of test configuration for a bitumen butt joint, (c) Experimental arrangement for a butt joint test in corn syrup.

defined as

$$\dot{\varepsilon}_T = \dot{\varepsilon} \exp\left(\frac{-Q}{R}\left(\frac{1}{T_1} - \frac{1}{T_0}\right)\right), \qquad (2)$$

where an experimental result obtained at a strain rate of $\dot{\varepsilon}$ and a temperature T_1, is shifted to a temperature-compensated strain rate $\dot{\varepsilon}_T$ at a reference temperature T_0.

Fracture energy per unit volume or 'normalised toughness' $G/2h$, is plotted against $\dot{\varepsilon}_T$ (over fifteen decades of temperature-compensated strain rate), in Fig. 3a. (See [22] and [23] for discussion on the use of

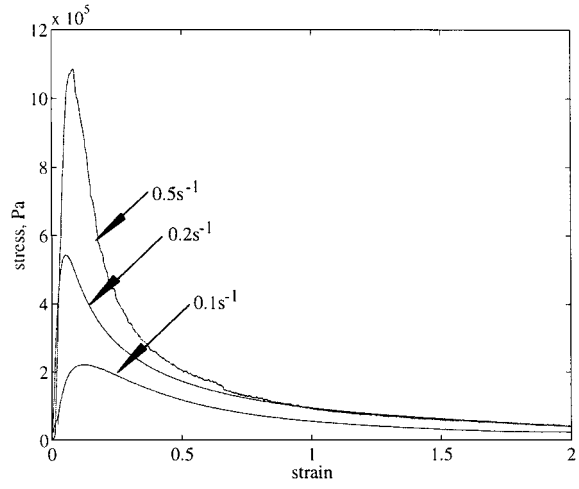

(a)

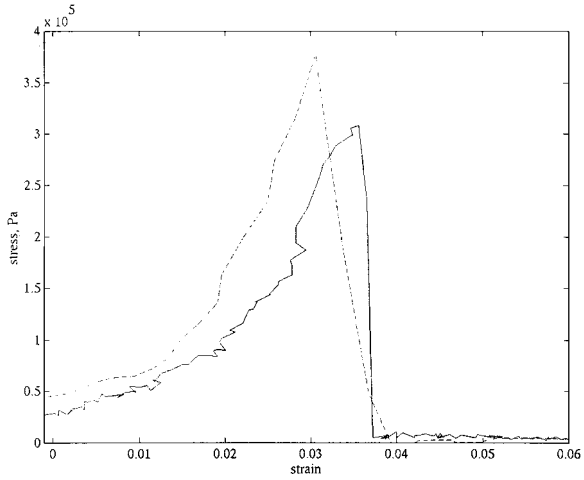

(b)

Figure 2 (a) Stress-strain curves for bitumen butt joints tested in the ductile regime at 20°C, (b) Stress-strain curves for bitumen butt joints tested in the brittle regime, at −30°C.——test at 0.1 s^{-1}; - - - - - - - - test at 1 s^{-1}.

TABLE I Material properties and parameter values for rheological model of bitumen

Reference stress $\sigma_{02} = 10^6$ Pa (measured uniaxially) $\sigma_{03} = 0.1\sigma_{02}$	Reference strain rate $\dot{\varepsilon}_{02} = 3.89\ s^{-1}$ (measured uniaxially) $\dot{\varepsilon}_{03} = \dot{\varepsilon}_{02}$
Power law exponents $n_2 = 1.5$ (measured uniaxially) $n_3 = n_2$	Elastic moduli $E_1 = 0.54$ GPa (measured acoustically) $E_3 = E_1/25$
Activation energy $Q = 245\ kJmol^{-1}$	Critical aspect ratio $A^* = 5.6\ \dot{\varepsilon}_{02}^{-0.02}$
Universal gas constant $R = 8.314\ Jmol^{-1}K^{-1}$	

this quantity as a failure criterion). The corresponding strain at failure is shown in Fig. 3b.

There are three main regimes of behaviour: ductile, brittle and transition.

(i) In the *ductile* region the normalised toughness (fracture energy per unit volume) is independent of film thickness, and increases with strain rate, i.e. the data points all fall on the same line of $G/2h$ vs $\dot{\varepsilon}_T$. The failure strain is constant at a value of approximately 2.6. This is consistent with a 'crack bridging' model of the fracture process, in which the fracturing material is modelled by crack bridging units, each having the behaviour of a simple bitumen film in tension. The fact that the normalised toughness is independent of film thickness implies that thicker films contain longer bridging units which display the same stress-strain response as their shorter counterparts.

(ii) In the *brittle* region the critical strain energy release rate G_{IC} is independent of strain rate. Consequently, the normalised toughness $G/2h$ depends on the film thickness, and hence is shown as a shaded band). The failure strain is also rate-independent, taking a value of approximately 0.04. This behaviour is characteristic of most brittle elastic solids.

(iii) In the *transition* region, the failure energy and strain vary from their values in the ductile regime to those in the brittle regime. There is some scatter in the results, due to the sensitivity of the fracture process to flaw size.

The dependence of fracture energy $G/2h$ on strain rate can be explained by recalling the rate-dependence of failure stress in the ductile region, and the rate-independence of fracture stress in the brittle region (Fig. 2). The fracture energy for a butt joint is the integral under the stress-strain curve to failure. It is not surprising that the fracture energy should follow a similar trend to the fracture stress when the failure strain is constant, since the stress in the film is largely independent of the aspect ratio for these specimens, as noted in the introduction.

3. Rheology

3.1. Uniaxial model

A rheological model consisting of Maxwell and Voigt elements in series, based on linear springs and non-linear (power-law) dashpots, was found to provide a reasonable representation of the uniaxial loading behaviour of bitumen. The model is sketched in Fig. 4. The governing equations defining the individual elements are as follows:

$$\text{Series dashpot} \quad \dot{\varepsilon}_2 = \dot{\varepsilon}_{02}\left(\frac{\sigma}{\sigma_{02}}\right)^{n_2} \tag{3a}$$

$$\text{Parallel dashpot} \quad \dot{\varepsilon}_3 = \dot{\varepsilon}_{03}\left(\frac{\sigma_{3d}}{\sigma_{03}}\right)^{n_3} \tag{3b}$$

$$\text{Series spring} \quad \dot{\varepsilon}_1 = \frac{\dot{\sigma}}{E_1} \tag{3c}$$

$$\text{Parallel spring} \quad \dot{\varepsilon}_3 = \frac{\dot{\sigma}_{3s}}{E_3} \tag{3d}$$

By adding the strains and strain rates for the series elements, and adding the stresses for the parallel elements, the governing equation for the system can be derived [22]:

$$\frac{\ddot{\sigma}}{E_1} = \ddot{\varepsilon} - \alpha n_2 \dot{\sigma}\sigma^{(n_2-1)} + \frac{\left[\dot{\varepsilon} - \dot{\sigma}\left(\frac{1}{E_1}+\frac{1}{E_3}\right) - \alpha\sigma^{n_2}\right]}{\left[\frac{1}{n_3 E_3}\beta\left(\dot{\varepsilon} - \alpha\sigma^{n_2} - \frac{\dot{\sigma}}{E_1}\right)^{(1/n_3-1)}\right]}, \tag{4}$$

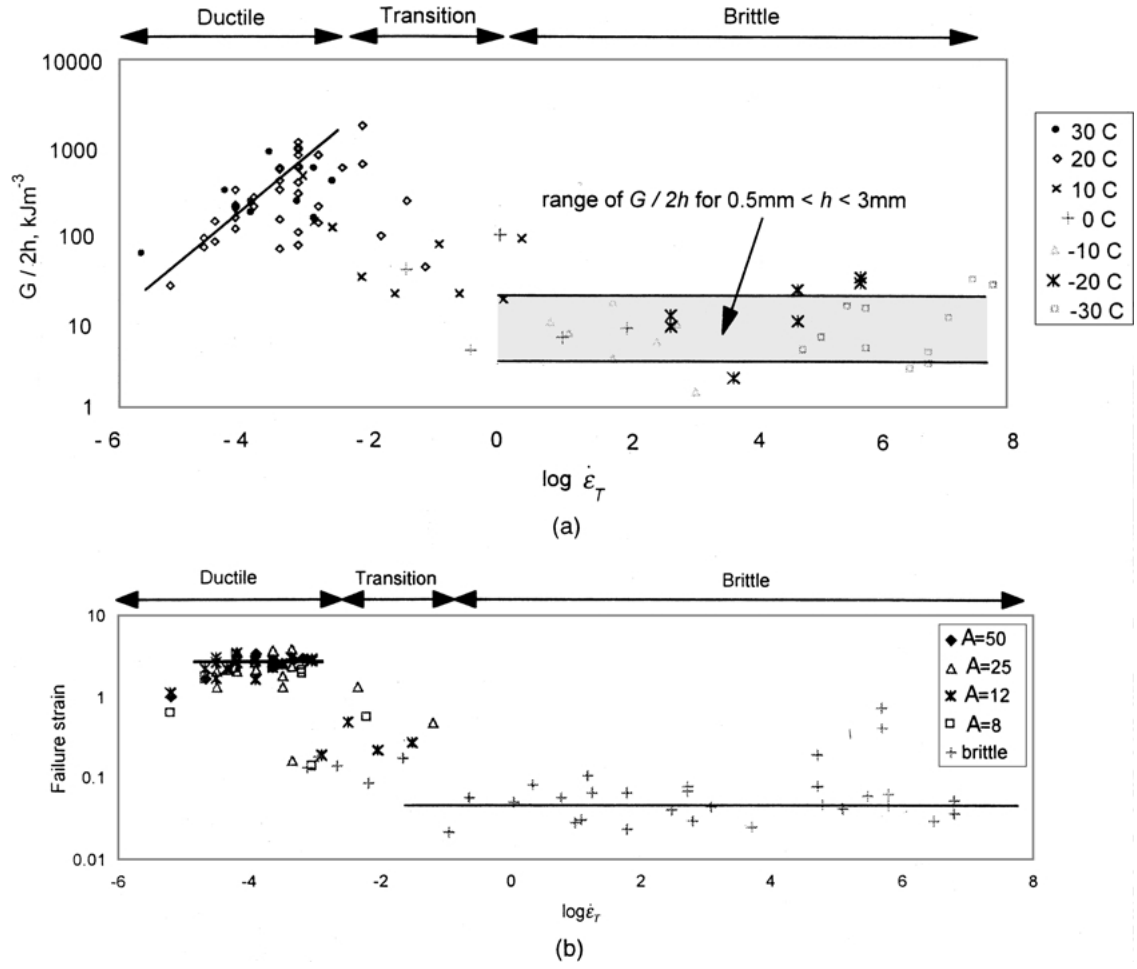

Figure 3 Performance of bitumen butt joints over a wide range of temperatures and strain rates. (a) Fracture energy, (b) Failure strain.

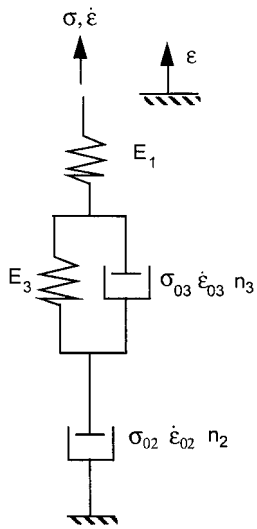

Figure 4 Sketch of 4-element spring-dashpot rheological model.

where α and β are material constants defined by:

$$\alpha = \frac{\dot{\varepsilon}_{02}}{\sigma_{02}^{n_2}}, \quad \beta = \frac{\sigma_{03}}{\dot{\varepsilon}_{03}^{1/n_3}},$$

and $\dot{\varepsilon}$ is the constant nominal strain rate applied to the system.

Numerical integration was performed to determine the stress-strain curve predicted by this model. The parameter values in the model were derived from uniaxial tests. Table I lists the material properties, and fitted model parameters. A comparison between uniaxial experiment and the model shows its suitability (Fig. 5).

3.2. 'Thick' film model

The stress response of a 'thick' bitumen butt joint of low aspect ratio (8 or less) in the ductile region of behaviour,

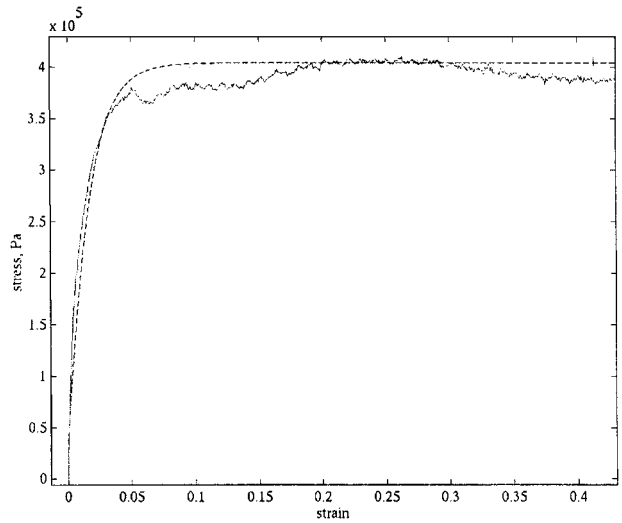

Figure 5 Comparison of 4-element theoretical model and uniaxial experiment at a strain rate of 1 s^{-1} and temperature of 20°C.———uniaxial experiment; - - - - - - - - Equation 4.

can be predicted by an extension of the small strain uniaxial model above. As the strain levels in the tests exceeded 100%, it was necessary for the small strain solution to be extended to large strains, by assuming a constant nominal strain rate. This large strain model allowed for the geometrical stiffening due to confinement of the film by the adherends as well as softening observed due to conservation of volume at large strains. Thick specimens were found to fail by rupture in the ductile regime.

The instantaneous true strain rate $\dot{\varepsilon}$ in Equation 4 is given by

$$\dot{\varepsilon} = \frac{\dot{\varepsilon}_n}{1 + \varepsilon_n}, \tag{5}$$

where $\dot{\varepsilon}_n$ is the nominal strain rate, and ε_n is the nominal strain.

Bitumen butt joints with rectangular plan area of 500 mm^2 were modelled as axisymmetric joints having this area of adhesive. Volume conservation was assumed, and a constant nominal strain rate was applied to the model.

The series dashpot (Fig. 4) was modified using a model of the non-linear viscous behaviour of a viscous film confined between moving rigid plates by Cheung and Cebon [6]. This involved the inclusion of an analytical stiffening factor, ψ_s. The nominal stress $F/(\pi r_0^2)$ applied to the film is a function the nominal strain rate $\dot{h}/h$ according to:

$$\left(\frac{F/(\pi r_0^2)}{\sigma_0}\right) = \psi_s \left(\frac{\dot{h}/h}{\dot{\varepsilon}_0}\right)^{\frac{1}{n}}. \tag{6}$$

Here the thin film stiffening factor is,

$$\psi_s = \left(\frac{n}{3n+1}\right)\left(\frac{n+2}{2}\right)^{\frac{1}{n}}\left(\frac{A}{\sqrt{3}}\right)^{\left(\frac{n+1}{n}\right)}, \tag{7}$$

where A is the aspect ratio of the film $A = b/h$, for a film of width b and thickness h. Thus, in Equation 4 above,

$$\alpha = \frac{\dot{\varepsilon}_{02}}{(\psi_s \sigma_{02})^{n_2}}. \tag{8}$$

This model applies when the film is thin, i.e. for aspect ratios $A \geq 8$.

For films thicker than $A = 8$, an interpolation is needed between the thin film solution and the uniaxial case ($A \leq 0.5$), so that the stiffening factor approaches unity for uniaxial specimens. The form chosen was

$$\psi_{sf} = \left(\frac{A}{A_0}\right)^{\left(\frac{n+1}{n}\right)} + 1, \tag{9}$$

where A_0 is a reference aspect ratio, having a value of $A_0 = 3.1$.

A comparison between the prediction of this 4-element thick film model and the measured stress-strain response of bitumen films with aspect ratios 2 and 5 is shown in Fig. 6. The softening behaviour at large strains is due to the formation of voids, which were observed in these specimens. The figure illustrates that the model predictions are reasonable over a range of aspect ratios.

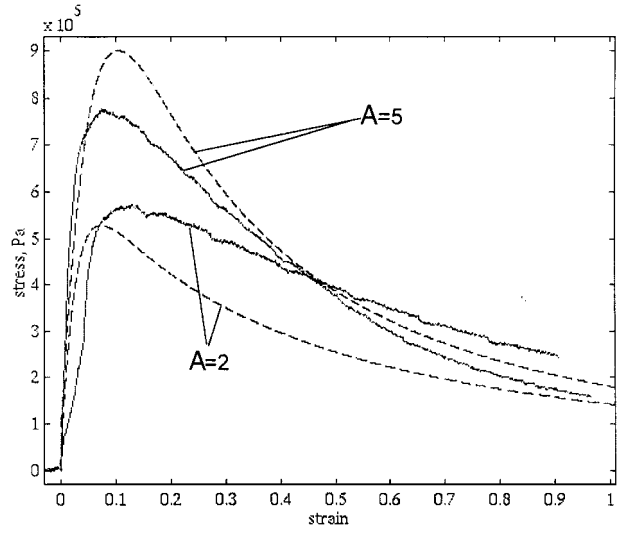

Figure 6 Comparison of 4-element model and experiment for specimens of aspect ratio 2 and 5, tested at 1 s^{-1} and temperature of 20°C. ——— experiment; - - - - - - - thick film model.

4. Ductile behaviour of thin films

4.1. Failure mechanisms in bitumen

Three main ductile fracture mechanisms were identified in bitumen, based on evidence from the fracture surface and the peak stress response.

(i) Flow, in which no voiding was observed, occurred in specimens with low aspect ratios. This failure mechanism was modelled in the previous section, and is referred to as the 'Flow I' mechanism.

(ii) Another flow mechanism, 'Flow II', was seen in specimens of higher aspect ratio, where any voids which formed did not leave evidence on the final fracture surface. This mechanism was seen mainly at the lowest strain rate, 0.01 s^{-1}. Tests on two different bitumens with different properties, confirmed that this regime is characterised by an increase in peak stress with aspect ratio. Neither the flow model of the previous section, nor that of Cheung and Cebon [6] for thin film flow, was found to fit this stress-strain behaviour. This mechanism is discussed further in Section 4.2.

(iii) The third mechanism was voiding, observed in high aspect ratio tests. In these specimens, there was evidence of void coalescence, although this process often occurred in conjunction with some inwards flow.

A mechanism map classifying failure of thin films is presented in Fig. 7 for data at 20°C: a temperature chosen to cover the range of ductile failure mechanisms at convenient strain rates. This map shows contours of strain rate on axes of failure stress and aspect ratio. It illustrates the region of dominance each failure mechanism.

In the *Flow I* regime, the peak stress increases with aspect ratio, as expected for a film. In the *Voiding* regime, the peak stress is independent of the aspect

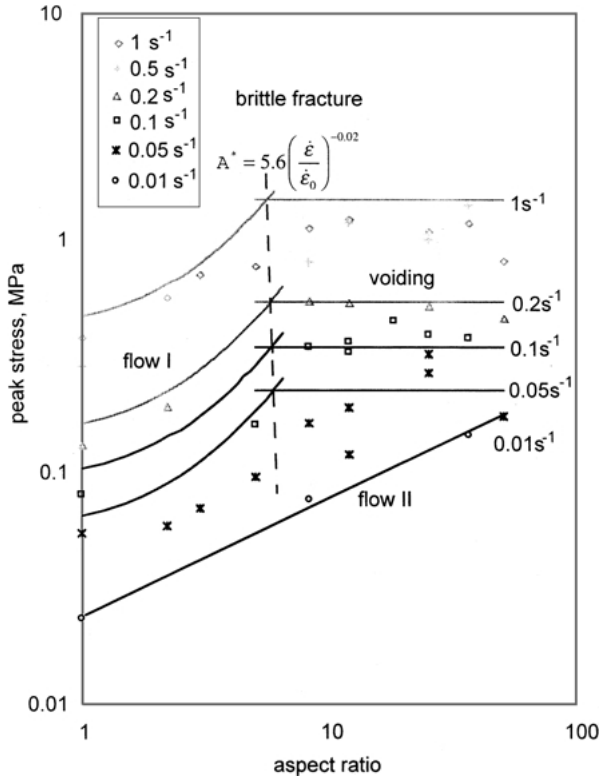

Figure 7 Thin film map showing failure mechanisms in bitumen.

ratio. This occurs for aspect ratios in the range 8–50. The *Flow II* regime shows different behaviour to the other two.

Fig. 8 shows a graph of peak stress plotted as a function of the strain rate, in the *Voiding* regime, and compares the results with the uniaxial behaviour. The points for aspect ratios of 8, 25 and 50 all fall on the same 'thin film' line. The peak stress displays similar power-law dependence on strain rate to the uniaxial behaviour, with the addition of a simple correction constant ψ_{sv}. The fitted equation for the film in Fig. 8 was used to plot the positions of the horizontal lines (at strain rates

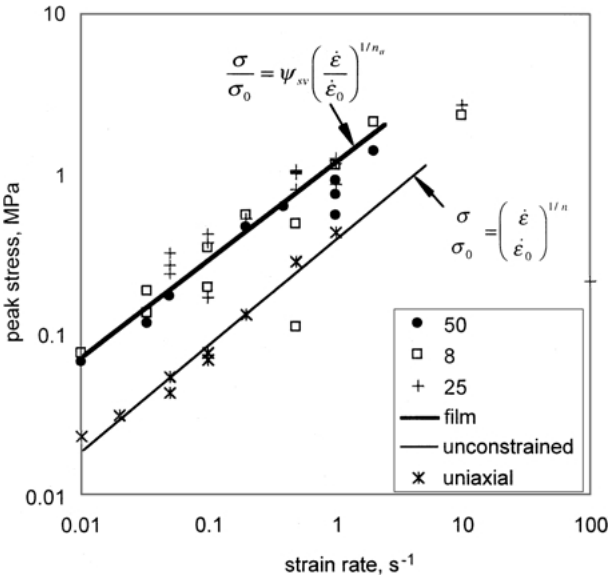

Figure 8 Comparison of peak stresses in tensile tests on bitumen at 20°C.- - - - - - - thin films;———uniaxial specimens.

of 0.05 s^{-1}, 0.1 s^{-1}, 0.2 s^{-1} and 1 s^{-1}) in the *Voiding* regime in Fig. 7.

The boundary between the *Flow I* and *Voiding* mechanisms in Fig. 7 is defined by a critical aspect ratio, A^*. The A^* boundary is governed by the intersection between the stress predicted by the thick film model in the *Flow I* region of the map, and the average peak stress at each strain rate in the *Voiding* region (as predicted from the fitted equation in Fig. 8). The value of A^* deduced for this bitumen, is shown as a dashed line on Fig. 7. It is slightly rate dependent.

A critical strain rate marks the boundary between ductile and brittle fracture in Fig. 7. This is approximately 2 s^{-1} for this bitumen. The boundary between *Flow II* and *Voiding* is also governed by a critical strain rate, approximately 0.03 s^{-1}.

Tests on corn syrup provide further insight into the voiding process. These are described in the next section.

4.2. Failure mechanisms in corn syrup

Tests on corn syrup (Fig. 1c) enabled visualisation of the voiding and flow process with simultaneous measurement of the stress-strain curves. The technique involved the attachment of a trigger light to the tensile testing machine. The light was photographed (on video) at the same time as the deforming specimen. This enabled loading and photographic data to be synchronised. These tests revealed that voids nucleated early in the test, well before the stress reached its peak.

Fig. 9 shows the sequence of events for a corn syrup film which failed by voiding. One flaw was initially visible. The voids shown in Fig. 9a became visible early in the test (point (a) on the curve), and began to coalesce at the peak of the stress-strain curve: point (b) and Fig. 9b. The voids ultimately coalesced and covered most of the area of the film as the load dropped to zero: point (c) and Fig. 9c. Although some cavities were often present in the initial unloaded film, these did not always begin to expand. Voids often suddenly appeared in an apparently non-voided fluid. It appeared that the nucleation stress was low (considerably lower than the yield stress), so that when voids nucleated, the event occurred early in the test.

At lower strain rates and aspect ratios, a flow mechanism was observed, in which fingers of material moved in from the edges of the axisymmetric film, Fig. 10. This mechanism was classified as "viscous fingering" [18, 21]. Inward flow begins at the point of peak stress: Fig. 10b. The fingers eventually expand to cover most of the area of the specimen, Fig. 10d.

A map summarising the failure mechanisms observed in corn syrup films is presented in Fig. 11. The map is similar to that for bitumen in Fig. 8, showing regions of voiding, viscous flow without fingering, and viscous fingering. The stress in the voiding regime is independent of aspect ratio, as for bitumen. However the aspect ratios at which voiding begins are consistently larger than for bitumen, because the corn syrup has a much lower viscosity. A comparison of the two maps suggests that the Flow II mechanism in bitumen is analogous to viscous fingering in corn syrup and can be

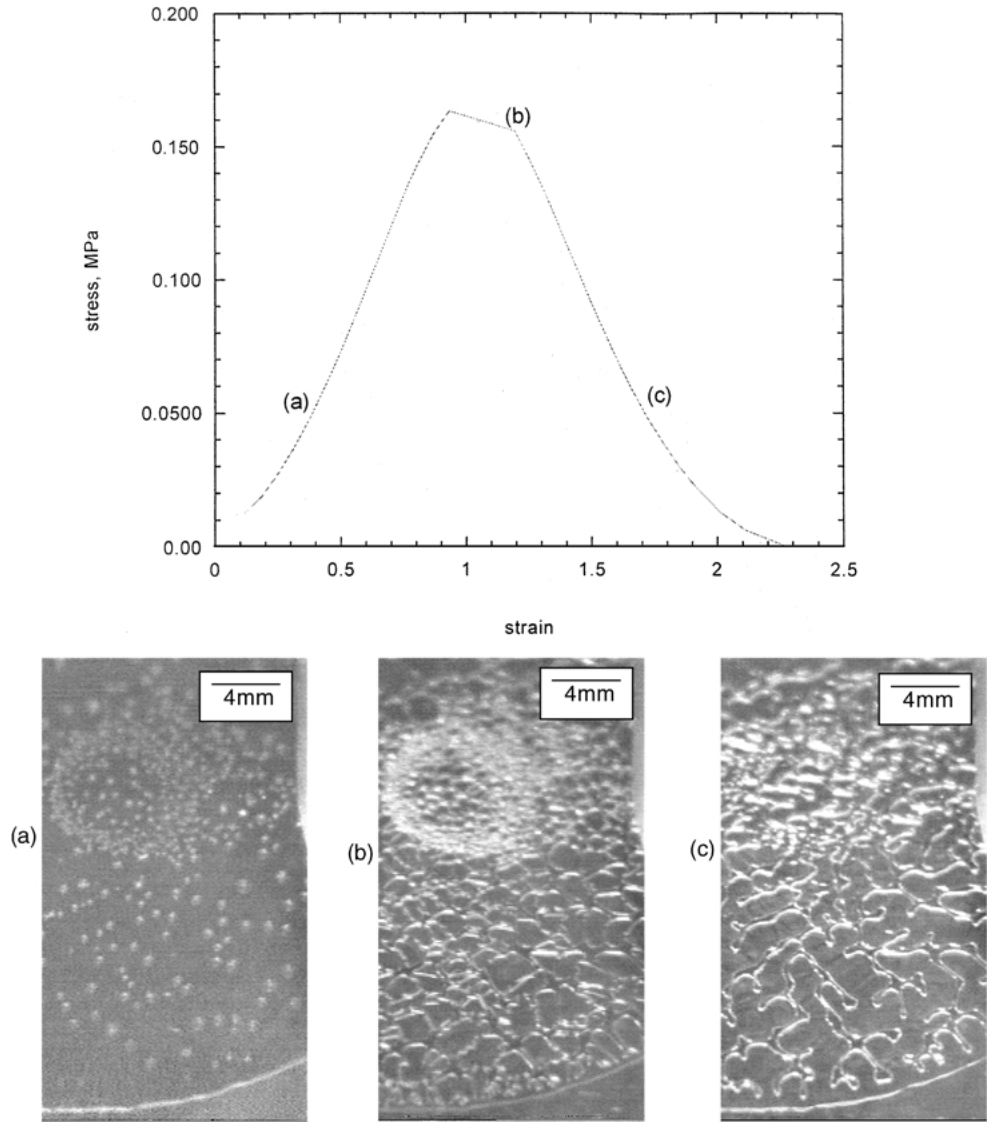

Figure 9 Failure of a corn syrup film by void coalescence.

characterised by the fact that the boundary of the film becomes severely distorted at failure. Note, however, that examination of the failure surfaces of the bitumen films did not provide conclusive evidence that Flow II was viscous fingering.

5. Model of voiding behaviour

During testing of bitumen in the voiding regime, voids coalesced to form ligaments of material. These ligaments continued to deform by viscous flow to ultimate failure. After separation of the adherends, the ligaments remained on the fracture surface, as the photograph in Fig. 12 illustrates. This observation is the basis for the voiding model presented here.

5.1. Number of voiding units

The critical aspect ratio can be used to estimate the effective number of patches of voiding material ("voiding units") under any conditions of temperature or strain rate. To achieve the aspect ratio-independence of stress observed in the voiding regime, (Figs 7 and 8), it is hypothesised that butt joint films effectively divide into units having the critical aspect ratio. Each such unit is assumed to contain one void. The following calculation scheme predicts the number of patches or ligaments, based on the critical aspect ratio.

An axisymmetric specimen, Fig. 13a, with the critical aspect ratio A^*, has radius r_0^* and thickness $2h^*$ such that

$$A^* = \frac{r_0^*}{h^*}. \tag{10}$$

An axisymmetric film, Fig. 13b, having radius r_0 and thickness $2h$ has aspect ratio,

$$A = \frac{r_0}{h}. \tag{11}$$

It is assumed that during the voiding process the film effectively subdivides into N units each having the critical aspect ratio. The ligament radius is r_0', Fig. 13c, where

$$A^* = \frac{r_0'}{h}. \tag{12}$$

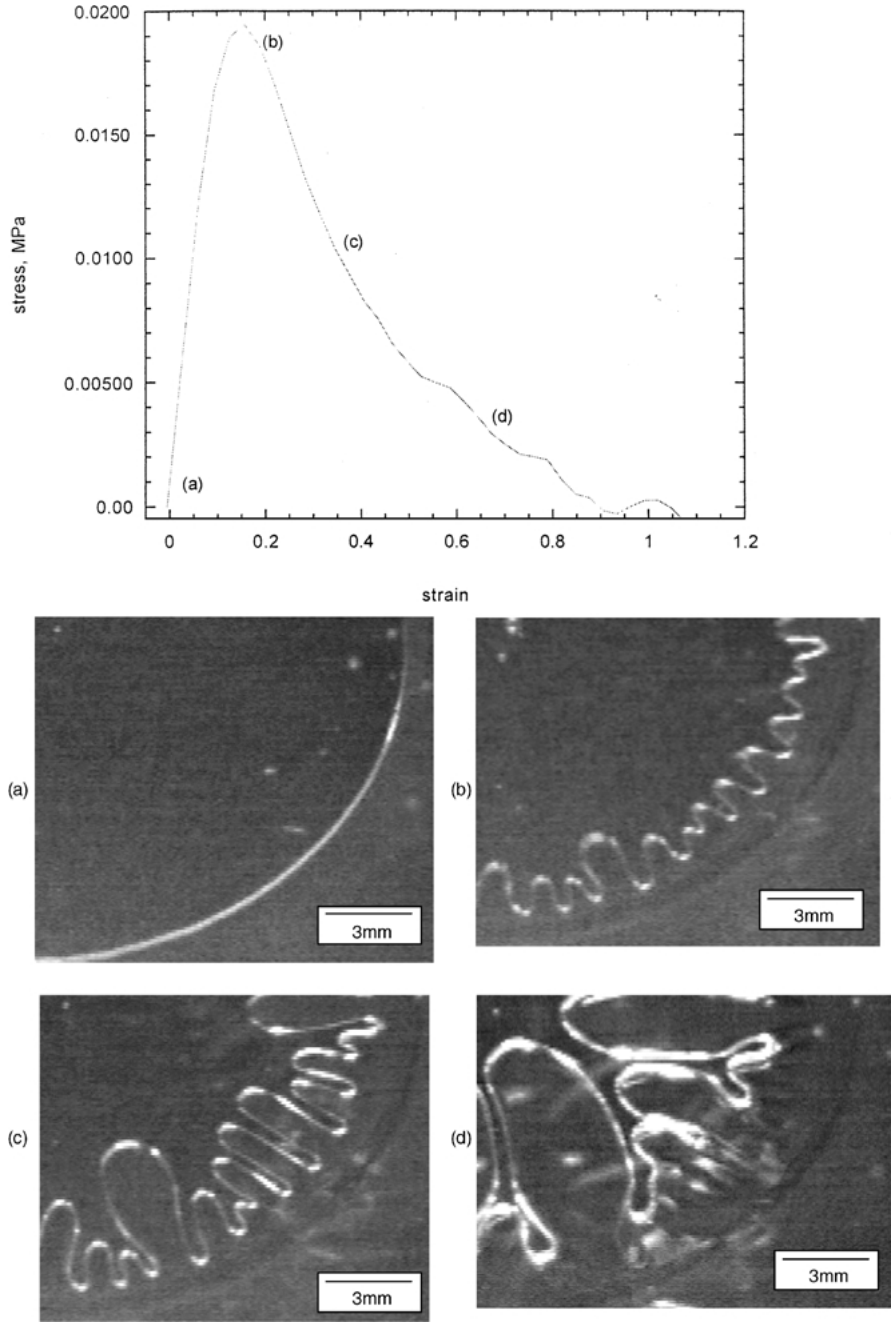

Figure 10 Failure of a corn syrup film by viscous fingering.

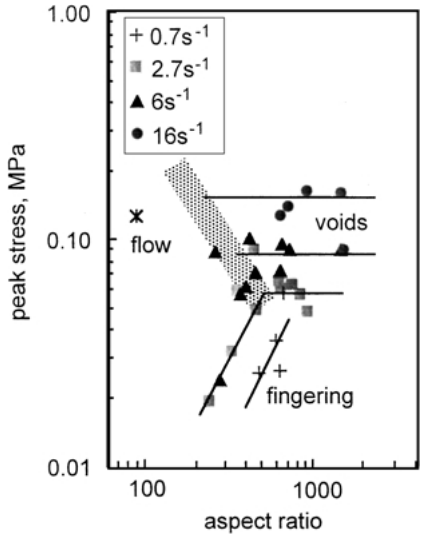

Figure 11 Failure mechanism map for corn syrup films in tension.

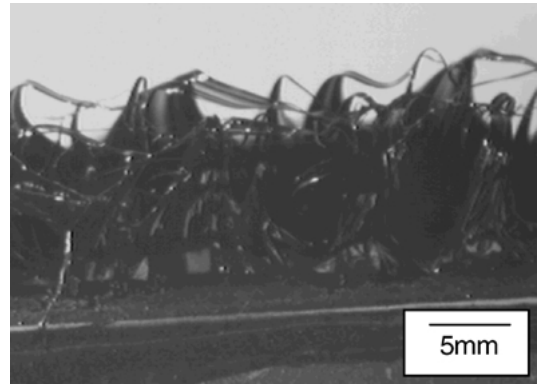

Figure 12 Photograph showing ligaments remaining behind on a fracture surface in bitumen.

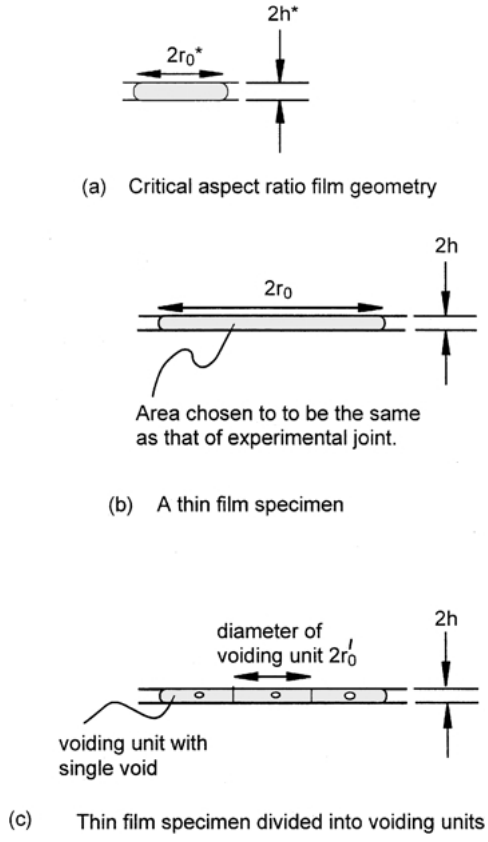

Figure 13 Division of thin film into voiding units.

Therefore,

$$r_0' = \frac{hr_0^*}{h^*} \tag{13}$$

Assume that the N units occupy the same area as the original film. Then the ratio of the area of an axisymmetric specimen composed of N ligaments, to the area of the same one before voiding is

$$N = \left(\frac{r_0}{r_0'}\right)^2, \tag{14}$$

or, combining Equations 11 and 12

$$N = \left(\frac{A}{A^*}\right)^2. \tag{15}$$

N represents the number of voiding units in the viscoelastic models of voiding discussed next.

5.2. Behaviour of voided film

The voided film was modelled as a number of separate voiding units, each having the critical aspect ratio. The number of ligaments N was determined based on the original geometry. Near the peak of the curve (where the series dashpot in the 4-element model (Fig. 4) dominated the response) the film was divided up into a number of ligaments or columns each with the critical aspect ratio. At the edge of each 'patch' or ligament, there is a void and the hydrostatic stress drops to zero. The ligaments therefore carry less stress between them than would an undamaged film at the same strain. They corresponded to the ligaments which were seen during testing, Fig. 12.

A four-parameter spring-dashpot system was used to model the voided film. No attempt was made to refine the elastic/delayed elastic part of the 4-element model, which remained independent of aspect ratio. A Poisson's ratio of 0.5 was assumed. The volume change associated with cavitation did not violate this assumption, since the model represented the ligaments between the voids. Voids were allowed to grow by viscous flow of the ligaments between them, and the area fraction of voids was idealised as filling the space between the ligaments. As before, a constant nominal strain rate was applied to the system.

The value of N was determined from the critical aspect ratio, using Equation 15. This was used to create a number of 'patches' of radius r_0' (Equation 14). All other parameter values remained the same as in Table I. A numerical integration was performed on a single patch since the average stress in one patch is representative of the stress carried by all the patches. Fig. 14 shows that there is quite good agreement between the model and experimental stress-strain curves.

A plot of the predicted normalised toughness, $G/2h$ against strain rate was made for films 0.5–3 mm thick. G was calculated from the area under the simulated stress-strain curves up to the known average failure strain. The film diameter chosen was equal to the width of the DCB specimen. The solid line on Fig. 15 shows a comparison between the model and experimental data from DCB tests. It can be seen that the model successfully predicts the values of $G/2h$ computed from measurements in DCB joints, over the range of strain rates and thicknesses tested. In the non-voided region (low strain rates) N is unity and the model reverts to the 'thick film' model described earlier. The model does not consider the packing of ligaments, or restrict the parameter N to integer values.

A refinement of this ductile fracture model might be to base the computations on a critical mean stress (e.g. a void nucleation stress), instead of the critical aspect

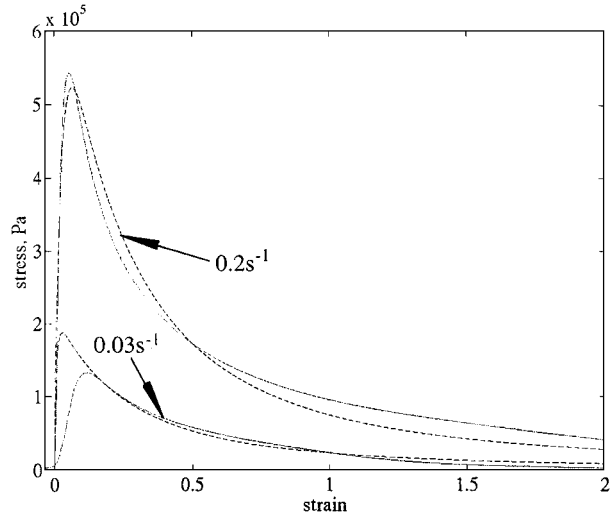

Figure 14 Stress-strain curves for voided film model and experiment. ———experiment;- - - - - - - model.

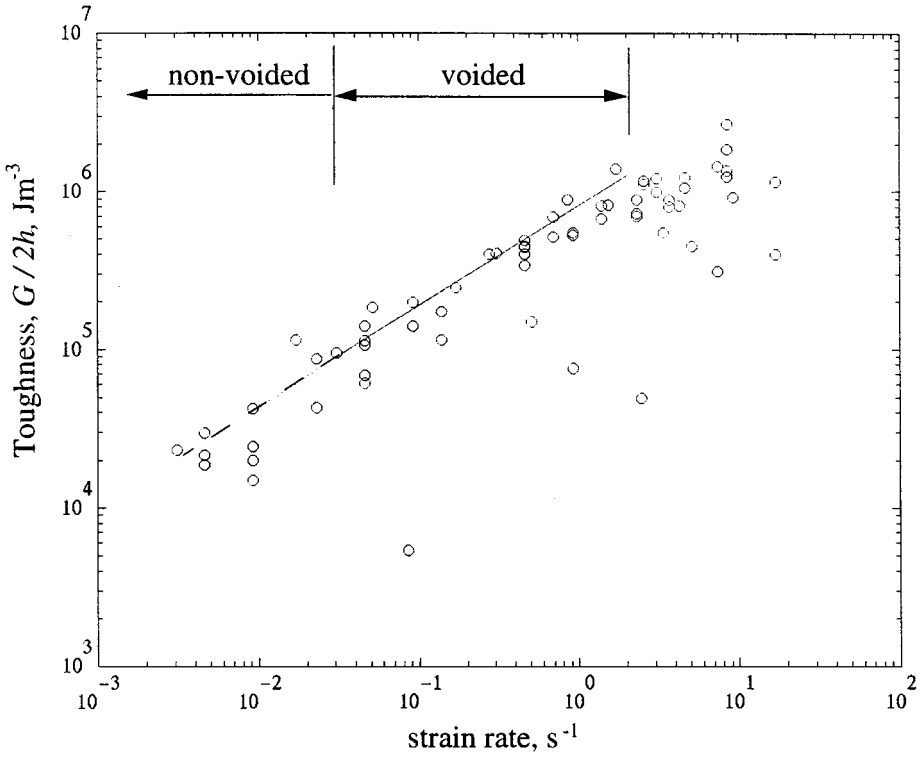

Figure 15 $G/2h$ calculated from voided film model and compared with DCB test results.

ratio. This would make the model more fundamental, allowing its application to other test geometries, however it would also require knowledge of the variation of the hydrostatic failure stress with strain rate and temperature. This is difficult to measure.

6. Voiding and brittle fracture

A failure mechanism map for bitumen films is shown in Fig. 16. It is based on the assumption that failure is governed by viscous flow or brittle fracture. It compares the failure stresses associated with the two mechanisms for various conditions of temperature and strain rate.

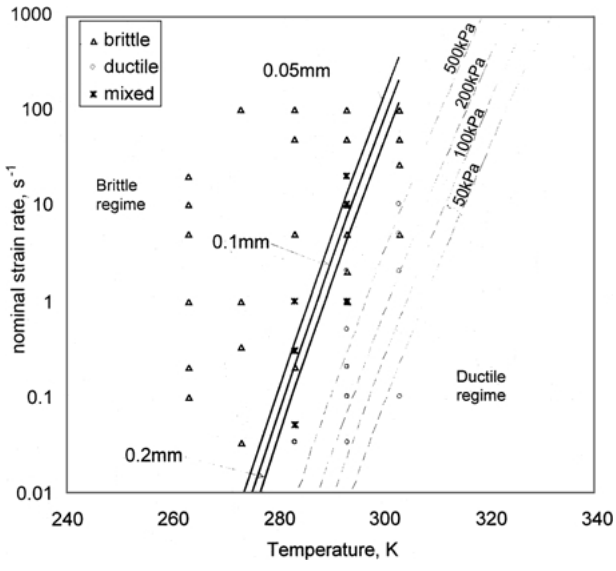

Figure 16 Failure mechanism map for bitumen films showing critical flaw sizes to induce brittle fracture, and contours of ductile failure stress.

The brittle fracture stress was calculated based on the estimate of G_{IC} obtained from butt joint tests, 10 Jm^{-2} [22, 23]. The equation is:

$$\sigma = \left(\frac{EG_{IC}}{\pi a}\right)^{\frac{1}{2}}. \tag{16}$$

where E, the Young's modulus, was measured at low-temperature and high frequency, using an acoustic method [22]. The critical flaw size, a was determined by equating the brittle fracture stress (Equation 16) with the failure stress in a power-law viscous film. The latter was calculated by increasing the uniaxial stress (Equation 1) with the thin film factor determined from the data in Fig. 8. This implies that the nominal strain rate is actually:

$$\dot{\varepsilon}_a = \frac{\dot{\varepsilon}}{\psi_{sv}^n}. \tag{17}$$

The value of the stiffening factor for a voided film ψ_{sv}, was determined from the results shown in Fig. 8, for this bitumen. $\dot{\varepsilon}$ is the strain rate in the uniaxial case, Equation 1.

In any bitumen film, there is a distribution of flaw sizes present. Both brittle fracture and void nucleation are affected by the largest flaw size within the film. Neither process will occur unless there are flaws above the certain size present. The viscous failure stress increases with falling temperature and rising strain rate, (Equations 1 and 17). Eventually, the failure stress exceeds some critical value, and brittle fracture occurrs. This brittle stress is associated with a certain critical flaw size. A line of critical flaw size therefore represents the boundary between ductile and brittle behaviour. Values

of critical flaw size a, were found to satisfy Equations 1, 16 and 17, so as to place these boundaries in the observed transition regime. These are plotted as lines of constant flaw size on the map (Fig. 16).

The map is realistic, although only a tensile stress field is considered, because the response of a voided film is well represented by a model having several patches, each of a low aspect ratio and relatively low hydrostatic stress. The direct strain is considerably greater than the transverse strain, which may be neglected.

7. Conclusions

(i) A non-linear, 4-element, spring-dashpot model gives a good representation of the tensile behaviour of thick films of bitumen.

(ii) Three general regimes of behaviour were observed in viscoelastic films: ductile, brittle and transition.

(iii) Within the ductile region, the failure mechanisms are voiding, thick film viscous flow (Flow I), and thin film viscous flow (Flow II), indicated by viscous fingering in corn syrup.

(iv) Voids nucleate well before the maximum stress is achieved in thin film specimens. The peak stress corresponds to the onset of void coalescence or inward flow.

(v) A comparison between the brittle fracture stress and the peak stress associated with voiding can be used to deduce a critical flaw size for brittle fracture.

(vi) A critical aspect ratio marks the boundary between voiding and thick film flow. A 4-element model of a film having a set of identical ligaments of critical aspect ratio can be used to represent the stress-strain behaviour of thin films.

(vii) The similarities in failure mechanisms for the two quite different viscoelastic materials tested here indicates that there is some generality in the qualitative conclusions of the investigation.

Acknowledgements

This work was funded by the Cambridge Commonwealth Trust, in conjunction with an ORS award, and the EPSRC. The authors are grateful to Professor Mike Ashby, Alan Heaver, Dr Vikram Deshpande and Dr Guy Genin for many useful discussions.

References

1. A. J. KINLOCH, *J. Mater. Sci.* **17** (1982) 617.
2. A. NADAI, "Theory of Flow and Fracture of Solids," Vol. 2. (Mc Graw Hill, New York, 1963).
3. B. P. HOLOWNIA, *J. Strain Analysis* **7**(3) (1972) 236.
4. N. L. HARRISON and W. J. HARRISON, *J. Adhesion* **3** (1972) 195.
5. A. H. COTTRELL, "The Mechanical Properties of Matter" (John Wiley, New York, 1964).
6. C. Y. CHEUNG and D. CEBON, *ASCE Journal of Engineering Mechanics* **123**(11) (1997) 1138.
7. R. K. PENNY and D. L. MARRIOT, "Design for Creep" (Chapman and Hall, London, 1995).
8. W. G. KNAUSS, *Advances in Fracture Research, ICF7* **4** (1989) 2683.
9. A. CHUDNOVSKY and D. B. SHULKIN, *J. Appl. Polym. Sci.* **56** (1995) 1465.
10. G. GENIN and D. CEBON, *Int. J. Road Materials and Pavement Design* **1**(4) (2000) 419.
11. P. KAKAVAS and P. J. BLATZ, *J. Appl. Polym. Sci.* **43** (1991) 1081.
12. P. A. KAKAVAS, *ibid.* **59** (1996) 251.
13. A. N. GENT and P. B. LINDLEY, *Proceedings Royal Society of London* A **249** (1959) 195.
14. P. J. BLATZ and P. KAKAVAS, *J. Appl. Polym. Sci.* **49** (1993) 2197.
15. R. D. ADAMS and J. COPPENDALE, *J. Adhesion* **10** (1979) 49.
16. D. CHEN and S. CHENG, *ASME Journal of Applied Mechanics* **57**(1) (1990) 78.
17. W. A. DUKES and R. W. BRYANT, *J. Adhesion* **1** (1969) 48.
18. P. G. SAFFMAN, and G. I. TAYLOR, *Proceedings Royal Society of London* A **245** (1958) 312.
19. G. I. TAYLOR and P. G. SAFFMAN, *Quarterly Journal of Mechanics and Applied Mathematics* **12** (1959) 265.
20. J. V. MAHER and J. IGNES-MULLOL, *Phil. Mag.* B **78**(2) (1998) 191.
21. R. J. FIELDS and M. F. ASHBY, *ibid.* **33**(1) (1976) 33.
22. J. A. F. HARVEY, "Bitumen films in tension" Ph.D. Dissertation (Engineering Department, University of Cambridge, 2000) p. 184.
23. J. A. F. HARVEY and D. CEBON, Proc. Int. Conf. on Asphalt Pavements, Copenhagen, 2002.

Received 6 November 2001
and accepted 31 October 2002